Original Article

Electrochemical corrosion behavior of Ti—35Nb—7Zr—5Ta powder metallurgic alloys after Hot Isostatic Process in fluorinated artificial saliva

Joan Lario[*], *Ángel Vicente Escuder, Francisco Segovia, Vicente Amigó*

Universitat Politècnica De València, Instituto De Tecnología De Materiales, Camino de Vera s/n, 5E Building, 46022, Valencia, Spain

ARTICLE INFO

ABSTRACT

The present study aimed to evaluate the effect of the Hot Isostatic Process (HIP) process on the microstructure, phase stability and corrosion resistance of Ti35Nb7Zr5Ta powder metallurgy alloys. The corrosion resistance of titanium alloys was tested by analyzing the open circuit potential (OCP), potentiodynamic polarization, electrochemical impedance spectroscopy (EIS), and ion release in physiological Fusayama solution. Polarization curves showed that the Ti—35Nb—7Zr—2Ta alloy presented good passivation behavior thanks to its low current densities ($<10^{-8}$ A/cm^2) and high polarization resistance. The interpretation of an equivalent electric circuit (EEC) demonstrated the formation of a very stable oxide film on the alloy, as indicated by good capacitive behavior, high impedance values ($>10^6$ Ω cm^2) at low frequencies and phase angles close to $-90°$ according to the EIS results with less ion release.

1. Introduction

Titanium alloys for dental implants undergo slow progressive corrosion in an oral environment. As the medium becomes more aggressive with more acid media or due to incorporated ions (F$^-$, Cl$^-$, SO$_4^{2-}$), oxide passive layer protective properties reduce or the degradation rate accelerates [1—3]. Titanium alloy lifetime expectancy depends on its mechanical properties, corrosion resistance and biocompatibility, which may continue to be suitable for a long service period, i.e. more than 30 years [4]. To meet these requirements, new titanium alloys require interdisciplinary efforts (materials science, industrial engineers, clinicians) to develop a manufacturing process, as well as surface treatments to acquire the required features to withstand long failure-free periods. Titanium alloy corrosion resistance is improved by adding beta-alloying elements, where tantalum is very resistant to acid dissolution, except for concentrated HF, and niobium and zirconium are highly passivating metals [5]. The conventional approach to increase titanium alloy corrosion resistance has involved adding alloying elements (V, Nb, Al, Mo) because microalloying enhances the cathodic and nobler corrosion potentials obtained in titanium alloys [6].

Titanium alloys' corrosion resistance very much depends on the environmental conditions (chemical composition, temperature, fretting) to which they are exposed, and also on the nature of their oxide surface [7]. For instance, solutions containing fluorine ions promote the dissolution of the titanium oxide layer [6]. TiO_2 dissolution in fluorine solution accelerates when temperature, ion concentration and electrochemical potential increase. Li et al. (2017) determined that the Ti CP passive film remains stable at a fluorine concentration below 0.03 M. When the amount of fluorine is increased, oxide film breakdown is activated and active dissolution is induced [6].

Metal alloys' adverse biological reactions depend on their corrosion resistance, and the *in vitro* evaluation is one of the first steps to characterize applicability for the biomedical field. The metal ions released as a result of corrosion or fretting may result in adverse biological reactions and lead to device failure. The study performed per Hussein et al. (2016) showed that Ti, Zr, Nb and Ta exhibit high biological biocompatibility, which make these β stabilizer elements suitable for use as materials for prostheses [8]. The modification of titanium alloys' corrosion resistance properties can be enhanced by adding highly passivating metals (Nb, Ta, Zr) because the oxides present on the alloy surface (ZrO_2, Nb_2O_5 and Ta_2O_5) strengthen the TiO_2 passive film [9,10].

The conventional route to manufacture titanium alloys is by completely melting all materials. For this purpose, vacuum heating technologies (Vacuum Induction Melting-VIM, Electron Beam Melting-EBM, and Vacuum Arc Remelting-VAR) are employed to produce billets or ingots. Unfortunately, these technologies have several drawbacks, mainly the high melting point of the constituent's elements (Ti at 1668 °C, Nb at 2477 °C, and Ta at 3017 °C), which implies a very high energy-use melting process to ensure complete melting and chemical homogeneity, and is directly associated with cost [11]. For titanium beta alloys, this involves a very high percentage of beta stabilization elements and several remelting steps to obtain the desired composition [12]. Powder metallurgy is an alternative processing route in which titanium alloy consolidation is obtained by sintering and diffusion. As the temperatures employed during sintering are far lower than the materials melting points, this method reduces the need for high energy-consuming melting and remelting systems. This technology also offers the advantage of titanium phases not depending on a liquids−solid equilibrium diagram because the consolidation process is achieved by a diffusion process. The conventional PM route starts with a powder mixture, cold pressing into the desired shape (green parts), and consolidation carried out by vacuum sintering to produce the part with 92−99% relative density [13]. The conventional PM production method is heavily introduced into the automotive industry for being a near-net-shape process that eliminates operations like machining and finishing, which drastically reduces the cost of parts.

In order to introduce PM titanium alloys into high-demand applications like aerospace and biomedical, an advanced metallurgical process (Mechanical Alloying-MA, Hot Isostatic Pressing-HIP, Cold/Hot Rolling or Drawing, and Equal Channel Angular Pressing-ECAP) should be introduced to eliminate residual porosity, homogenize the microstructure, reduce grain size, and improve fatigue and corrosion resistance [14−16]. Advance beta titanium alloys is cost challenging process because multiple remelting steps are required to homogenize the beta stabilizers into the titanium matrix (Nb, Mo, Ta, etc.). Powder metallurgic route, where porosity is practically eliminated hot isostatic pressing, is an appropriate manufacturing approach to overcome the current deficiencies present in melting manufacturing technologies.

The purpose of the present study is to compare the electrochemical properties of powder metallurgy Ti−35Nb−7Ta−5Zr alloys according to the process route, where different cooling rates are applied during the HIP process, where the alloys are immersed in fluorinated artificial saliva medium.

2. Methods

2.1. Processing conditions

The Ti−35Nb−7Zr−5Ta samples were prepared from commercial powders Ti CP (99.6 wt% HDH, $\leq$ 50 μm), Nb (99.9 wt%, $\leq$ 35 μm), Zr (99.9 wt%, $\leq$ 35 μm) and Ta (99.9 wt%, $\leq$ 35 μm), supplied by Atlantic Equipment Engineers (AEE Inc., USA). Powders were prepared in an argon chamber to avoid oxidation. To increase homogeneity, they were mixed in turbula equipment (Bioengineering, Switzerland). The green parts were obtained by a double-effect floating die press operating at 700 MPa pressure. The sintering process was performed in a tubular furnace at high-vacuum $<10^{-4}$ mbars (HVT 15/75/450, Carbolite Gero Ltd., UK). The sintering samples were prepared in two steps: in the first one, samples were heated to 800 °C (10 °C/min) and held for 1.8K seconds to homogenize. In the second step, samples were heated to 1350 °C (7 °C/min) for 10.8K seconds and furnace-cooled to room temperature ($\approx$10 °C/min). The post-processed HIPed samples were obtained under two different conditions (QIH21, Quintus Technologies AB, Sweden). The HIP parameters employed for the two scenarios are summarized in Table 1.

Standard ASTM C373-88 was applied to measure the relative density of each Ti−35Nb−7Zr−5Ta condition (conventional PM, HIP1 and HIP 2). Three-point bending tests, according to Standard ISO 3325, were carried out for mechanical characterization purposes (AG-X plus 100 kN,

Table 1 − The parameters selected for the Ti−35Nb−7Zr−5Ta processing step.

Processing route	Pressure (MPa)	Maximum Temperature (°C)	Time (minutes)	Cooling rate (°C/min)
Press and Sintering (PS)	N/A	1350	180	15
HIP 1 (Fast cooling)	150	1200	120	500
HIP 2 (Slow cooling)	150	1200	120	100

Shimadzu, Japan). Young's modulus was obtained by the impulse excitation technique (Sonelastic CA-DP, ATCP Engenharia Física, Riberao Preto-SP, Brazil).

2.2. Metallographic characterization

The optical microscopy analysis was performed on the polished samples to observe internal residual porosity (LV100, Nikon, Japan). Acid etching (Kroll reagent) was employed to reveal the titanium alloy phases according to the processing route. The metallographic analysis (grain size and crystal orientation, morphology and phase identification) was performed using a Field Emission Scanning Electron Microscope (FESEM, AURIGA Compact, ZEISS, Germany), an Energy Dispersive Spectroscope (EDS, Oxford Instruments Ltd., UK) and an Electron Backscatter Diffraction (EBSD) detector. The EBSD operated at 20 kV and 5 nA, and step size was set at 0.05 μm on a sample tilted 70° from the horizontal for orientation mapping.

2.3. Electrochemical characterization

The corrosion resistance evaluation for the powder metallurgy Ti–35Nb–7Zr–5Ta alloy was measured in a Fusayama electrolyte with NaF addition to simulate a dental implant's ambient conditions [6]. The chemical composition of Fusayama artificial saliva is summarized in Table 2. First 0.012 (mol/L) of NaF were added to simulate mouth rinses and dentrified conditions [2]. The electrochemical cell was set up as per a three-electrode system, where an Ag/AgCl saturated calomel electrode (SCE) was employed as the reference electrode, platinum sheet as the auxiliary electrode and a PM titanium alloy as the working electrode. To obtain a smooth homogeneous surface, titanium PM samples were ground to 2000 SiC finish, followed by distilled water washing and air drying before corrosion test measurements were taken. Samples were positioned on the corrosion cell by leaving a circular area of 0.75 cm^2, where the reference electrode was very close to the working electrode surface.

Electrochemical studies were conducted with the conventional PM and HIPed samples using potentiostat/galvanostat PGSTAT204 (Metrohm Autolab BV, The Netherlands). Samples were immersed in an Fusayama electrolyte for 30 min to establish the open circuit potential (OCP) or the steady state potential. After the OCP measurements, potentiodynamic polarization studies were performed within a potential range from OCP to +3000 mV (SCE) at a scanning rate of 0.2 mV/s. The electrochemical impedance spectroscopy (EIS) measurements were taken by applying an alternating sinusoidal potential of 10 mV to the OCP within the frequency range from 10 mHz to 100 kHz. The acquired EIS data were fitted and analyzed by the ZView program (version 3.5a from Scribner Associates Inc., USA) for the equivalent circuit simulation, quantification and parameter selection. Quality of fit was checked by the χ^2 value. The ion concentration for elements Ti, Nb, Zr and Ta after 730 h and 36–38 °C in fluorinated Fusayama artificial saliva, which simulated a 20-year exposure period [14], were measured by inductively coupled plasma optical emission spectroscopy ICP-OES analyzer VARIANT-715ES (Thermo Fisher Scientific, USA).

3. Results

Conventional powder metallurgical titanium alloys present several drawbacks, such as residual porosity and chemical homogeneity, which limit their use in orthopedic implants. The HIP post-process is capable of modifying the density and titanium phases because it is a thermo-mechanical process that adds plastic deformation and improves the diffusion of alloying elements. Densification is around 79% (green part) after the compaction process, and density increases to 96% after the sintering cycle. Finally after post-processing through HIP, full density of beta titanium samples is achieved (Table 3). Porous alloys present more surface area exposed to the media, larger surface makes more sensitive the titanium alloy to corrosion. Yilmaz et al. (2018) reported that the increment of porosity in the Ti–Nb alloys increases the corrosion current density, reduce the polarization resistance and accelerates the corrosion rate [17]. As the retained β phase percentage was above 50% at room temperature, the three processing conditions allowed classification in the β titanium alloys category.

Beta titanium alloys grain size and phases are factors that control mechanical properties and corrosion resistance. The acid etched Ti–35Nb–7Zr–5Ta samples are presented in Fig. 1 according to their powder metallurgic condition. The dark areas on the optical microscopy images reveal the presence of the α phase. As the sintered beta titanium alloy presented many α+β areas (Fig. 1A and D), the same phenomenon was observed in the HIP 2 samples, where the cooling rate was

---

Table 2 – Chemical composition of fluorinated Fusayama solution.

Element:	Urea	NaCl	KCl	CaCl$_2$	H$_2$PO$_4$	NaF	Na$_2$S
Concentration (g/l)	1.0	0.4	0.4	0.8	0.7	2.5	0.005

Table 3 – Archimedes' results and metallographic characterization of the Ti–35Nb–7Zr–5Ta alloy.

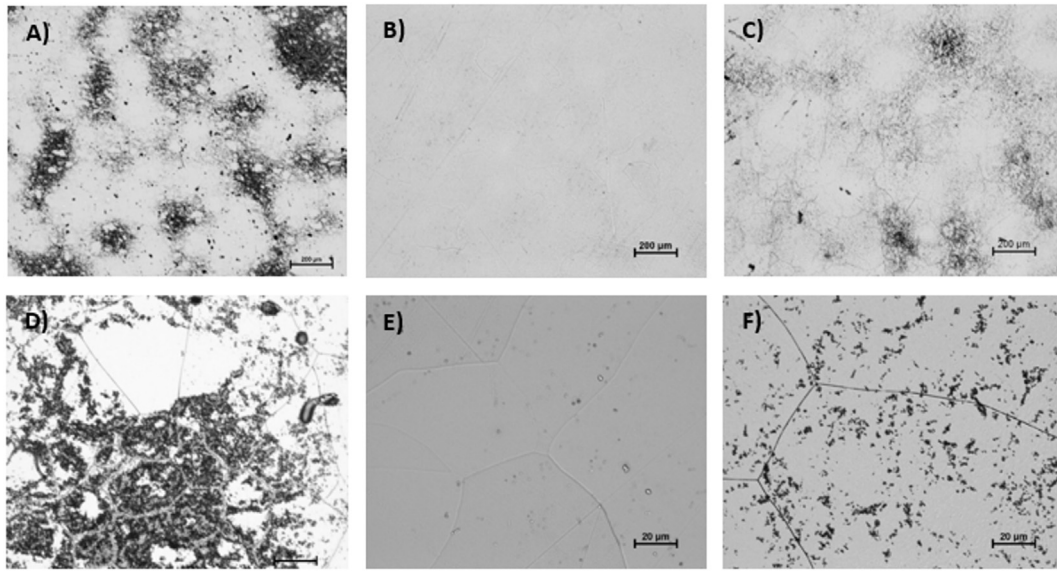| Material	Processing route	Green density (%)	Relative density (%)	Porosity (%)	β phase (%)	α+β phase (%)	Grain size (μm)
Ti–35Nb–7Zr–5Ta	Press and Sintering		96.0 ± 0.1	4.1	71.5	23.6	24 ± 11
	HIP 1 (Fast cooling)	79.4 ± 0.4	100.1 ± 0.1	0.4	98.7	0.7	48 ± 22
	HIP 2 (Slow cooling)		100.2 ± 0.2	0.2	89.3	10.5	74 ± 49

Fig. 1 – Metallography of the Ti–35Nb–7Zr–5Ta acid etched samples according to the manufacturing conditions. A) and D) Conventional vacuum sintering. B) and E) HIP 1 at 500 °C/min. C) and F) HIP 2 at 100 °C/min.

100 °C/min (Fig. 1C and F). HIP post-processing allowed the α phase amount to be reduced, where β equiaxial grains predominated (Table 3). The thermo-mechanical treatment above the beta transus temperature increased grain size (Table 3), and the 500 °C/min cooling rate practically permitted full beta phase retention (Fig. 1B and E). The SEM and EBSD analyses performed on the HIP 2 Ti–35Nb–7Zr–5Ta samples demonstrated that the previous α + β areas detected (Fig. 1) by optical microscopy were actually α" precipitates at the β matrix (Fig. 2B). The orthorhombic structure (α" phase) observed at HIP 2 (100 °C/min) resulted from α -martensite's hexagonal structure, which became distorted due to the large amount of

beta alloying present in the powder metallurgic titanium alloy.

In order to complete an effective HIP cycle, the selected temperature should be above the titanium beta transus temperature. When working within this range, yield stress reduces and diffusion efficiency is enhanced, which allows residual porosity to close in a reasonable time. Pore closure increased the percentage of ductility, and samples' ultimate tensile strength (UTS) was studied (Table 4). The microstructure influenced UTS and Young's modulus, as reflected by the lower standard deviation samples process through HIP 1, where higher β phase homogeneity was present. The fast-
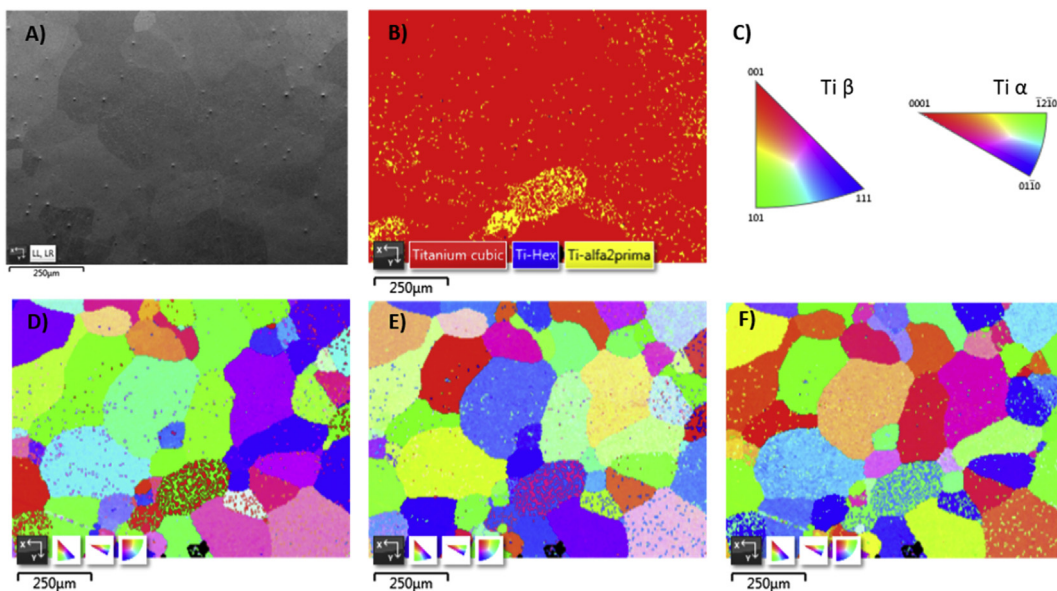

Fig. 2 – Microstructure of the Ti–35Nb–7Zr–5Ta after HIP2. (A) the SEM image. (B) images showing α" precipitates. (C) crystallographic orientation for the β and α" phases. (D–F) Inverse pole figures (IPF) for the X, Y, and Z reference direction maps highlighting grains.

Table 4 – Mechanical results of the Ti–35Nb–7Zr–5Ta alloy.

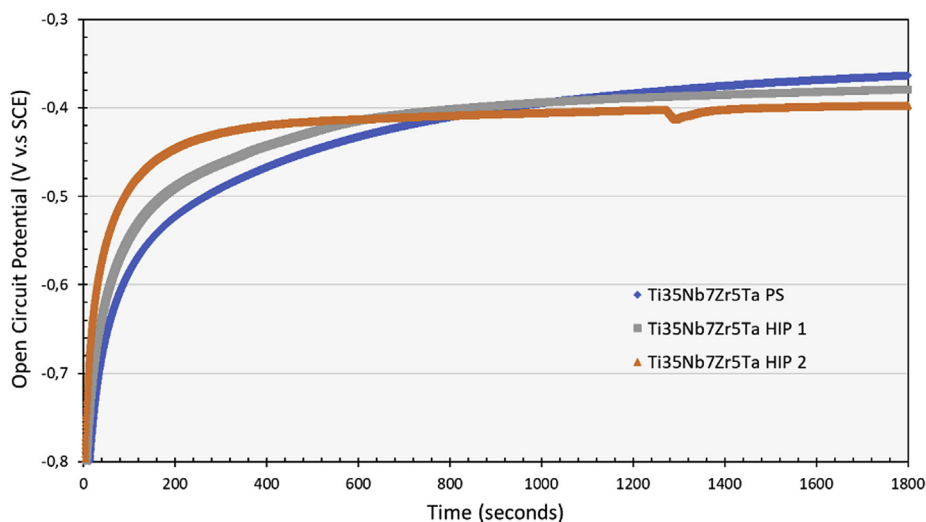| Material	Processing route	UTS (MPa)	ε (%)	E (GPa)	G (GPa)	Poisson's ratio
Ti–35Nb–7Zr–5Ta	Press and Sintering (PS)	910 ± 215	2.9 ± 0.1	79.8 ± 3.5	27.0 ± 1.2	0.4 ± 0.1
	HIP 1 (Fast cooling)	1058 ± 97	3.6 ± 0.4	76.8 ± 1.1	27.4 ± 0.4	0.4 ± 0.1
	HIP 2 (Slow cooling)	1219 ± 232	4.2 ± 0.9	77.6 ± 4.0	27.0 ± 1.2	0.4 ± 0.1

Fig. 3 – OCP evolution with time of the Ti–35Nb–7Zr–5Ta samples by their processing condition in Fusayama solution.

cooling rate of the HIP 1 samples (500 °C/min), together with the phase obtained thanks to its chemical composition, gave a Young's modulus below 80 GPa, which improved the current 100 or 110 GPa available for the Ti CP and Ti–6Al–4V alloys employed to manufacture implants. Titanium alloys with a low modulus diminish the stress shielding effect, minimize bone atrophy and enhance implant durability [18].

The OCP and current density for the Ti–35Nb–7Zr–5Ta alloys are represented in Fig. 3. Current beta titanium alloys reach their plateau current density at a potential of −0.3 V,

which indicates the formation of a highly passive layer in Fusayama solution, shown by less ion release than forging α and α+β titanium alloys. These values are similar to those reported by Schiff et al. (2002) and also obtained in Fusayama solution [2]. The continued increase in the corrosion potential indicated the passivation of the titanium alloys in this medium.

Figure 4 illustrates the potentiodynamic polarization curves recorded in Fusayama artificial saliva for Ti–35Nb–7Ta–5Zr under different processing conditions
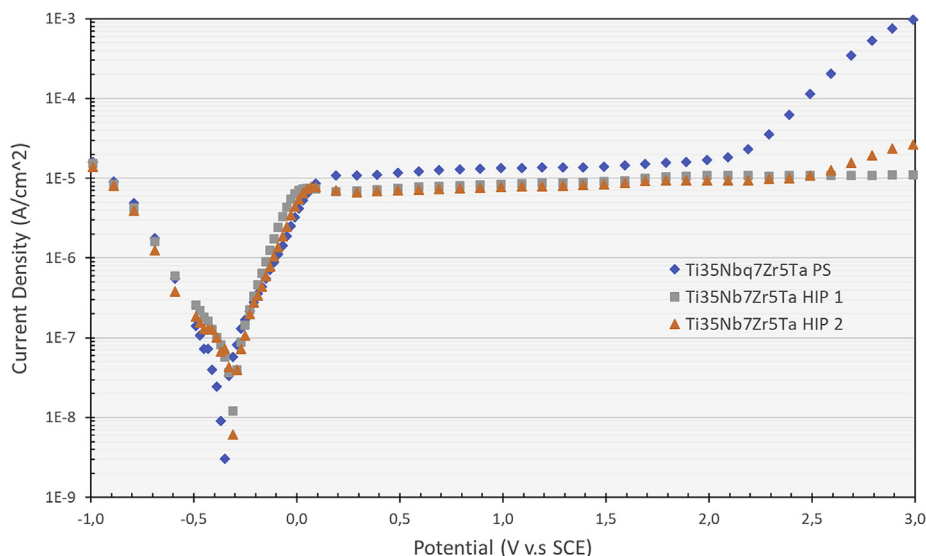

Fig. 4 – Potentiodynamic polarization curves of the Ti–35Nb–7Zr–5Ta samples according to their processing condition in Fusayama solution.

(conventional PM and HIPed). The current density manifested a marked increase of at least one order of magnitude in the conventional powder metallurgy and slow cooling HIPed samples (HIP 2) versus the high cooling rate HIPed sample (HIP 1). As shown in Fig. 4, both powder metallurgy Ti−35Nb−7Zr−5Ta alloys exhibit a wide passive plateau until the applied potential reached 2.5 VSCE without pitting or transpassivation. The lower current density is indicative of the protectiveness of passive film changes and reduces according to the cooling rate. A single β-phase was present in the beta Ti−35Nb−7Ta−5Zr alloy from the HIP 1 samples (Fig. 1B and E). The high cooling rate allowed the galvanic coupling effect to be eliminated as alloys are considered to be homogeneous solid solutions under these conditions. The HIP 1 processing condition displayed the greatest corrosion resistance behavior under the studied conditions given its present lowest corrosion rate and nobler corrosion potential (Table 5). Similar behavior has been reported by Atapour et al. (2011) about the TiOsteum and TMZF alloy under different heat treatment conditions, where the potential difference between the α and β phases creates galvanic coupling between them [9].

The calculated corrosion kinetic parameters as corrosion potential (E_{corr}), corrosion current density (I_{corr}), polarization resistance (PR) and passive current density (I_p) have been presented in Table 5. The nobler corrosion potentials found for Ti−35Nb−7Zr−5Ta (Table 5), compared to Ti−6Al−4V ELI and Ti CP, can be justified by more alloying content being added (Nb, Zr and Ta). These elements improved passivation behavior due to rich pentoxide development with higher corrosion resistance (i.e. Nb_2O_5 and Ta_2O_5) compared to the TiO_2 form for conventional titanium alloys [4,6,9,19,20]. The studied powder metallurgy alloys showed superior corrosion resistance than conventional titanium alloys (Ti CP and Ti−6Al−4V ELI), whose corrosion potential and corrosion current density are around −0.34 V and 9.98×10^{-8} A/cm^2 compared to −0.37 mV and 1050×10^{-8} A/cm^2 obtained by Schiff et al. (2002) [2].

The EIS results in fluorinated Fusayama solution are represented in Bode and Nyquist plots (Fig. 5A and B) or the different processing conditions (PS, HIP1 and HIP2) studied. Within the medium frequency range, high impedance (above 10^6 Ω cm^2) values were observed, typically from the passive material employed in biomedical devices. These results are consistent with the low current density and noble corrosion potential determined during polarization tests, which suggests that a high resistance film is formed on the beta titanium alloy surface.

At a low frequency, phase angles lowered to −65º, capacitive behavior decreased due to phase heterogeneity, and

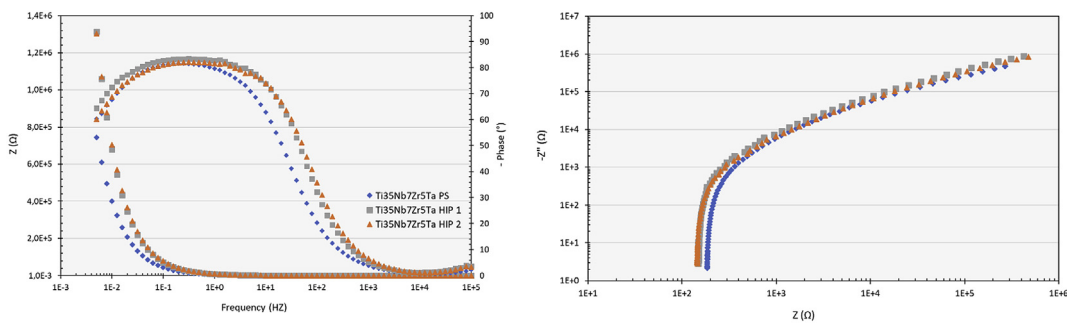| Table 5 − Corrosion parameters from polarization plots.							
Processing condition	OCP Global (V)	E_{corr} (V)	j_{corr} (nA/cm^2)	PR (MΩ)	I_{p1V} (µA/cm^2)	I_{p2V} (µA/cm^2)	I_{p3V} (µA/cm^2)
Press and Sintering (PS)	−0.33 ± 0.05	−0.34 ± 0.03	100 ± 70	0.8 ± 0.4	17.9 ± 0.2	22.6 ± 0.1	1281.9 ± 8.1
HIP 1 (Fast cooling)	−0.38 ± 0.01	−0.30 ± 0.02	65 ± 40	0.6 ± 0.1	10.5 ± 1.1	12.8 ± 0.2	14.0 ± 0.1
HIP 2 (Slow cooling)	−0.33 ± 0.10	−0.28 ± 0.08	75 ± 30	0.8 ± 0.3	10.1 ± 0.2	12.3 ± 0.1	30.9 ± 0.6

Fig. 5 − Electrochemical impedance spectroscopy measurements of the Ti35Nb7Zr5Ta samples under their processing conditions in Fusayama solution. A) Bode plots. B) Nyquist plots.
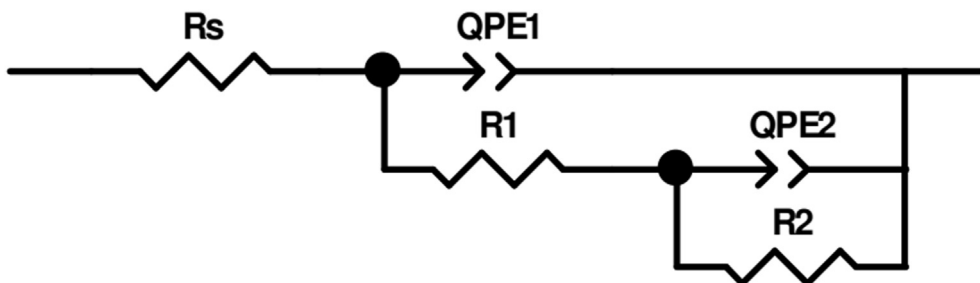

Fig. 6 − The two-time constant equivalent electrical circuit for the Ti−35Nb−7Zr−5Ta alloy.

electrochemical protectiveness diminished owing to galvanic coupling. The variation in the phase angles observed in the HIPed parts compared to the conventional press and sintering parts was related to reduced porosity, and also to the greater chemical and phase homogeneity obtained after thermo-mechanical treatment. Higher beta content involved better capacitive behavior. The Ti—35Nb—7Zr—5Ta postprocessed by HIPing at the higher cooling rate (500 °C/min) was employed and showed higher phase angles for all three studied conditions.

A two-time constants equivalent electrical circuit (EEC) was employed to fit the EIS experimental data (Fig. 6). The QPE elements were selected to simulate the experimental data and to consider non ideal behavior capacitors. The oxide that spontaneously formed on the Ti—35Nb—7Zr—5Ta alloy surface was considered to be formed by two layers: an outer porous layer in contact with saline solution; an inner layer in contact with the metal surface acting as a compact barrier. The two-time constants from the electrical model with the layers were given by parameters R1 and QPE1 (outer) and by R2 and QPE2 (inner). Fusayama solution was represented by Rs. The electrochemical parameters obtained after simulating the response of the EEC are summarized in Table 6. A good agreement between the experimental data and the simulated values was obtained with χ^2 values of the 10^{-3} order.

Table 6 summarizes the electrochemical parameters obtained to simulate and fit the Ti—35Nb—7Zr—5Ta oxide surface film EIS measurements to the proposed EEC (Fig. 6). The outer layer's (R1) electrochemical resistance was lower than it was for the inner layer. This scenario was observed by the low resistance average values (200—700 Ω cm^2) obtained for the three studied conditions. However, the inner oxide layer's electrochemical resistance was considerably higher, above 1.4 MΩ cm^2, which provided excellent corrosion resistance in Fusayama solution. The inner oxide layer's lower capacitance and higher resistance values restricted the movement of metal ions from the titanium alloy to Fusayama solution and fewer ions were released to media. The highest corrosion resistance of niobium compared to titanium has been demonstrated by Li et al. (2017) [6]. Yilmaz et al. (2018) observed the EIS that Ti-xNb alloys shifts to more capacitive and noble behavior, increment of the diameter in Nyquist diagrams, when the amount of Nb was increased [21]. Previous potentiodynamic polarization and EIS studies in beta titanium alloys are consistent with the current results [2,21—25]. The oxide layer developed on niobium (Nb$_2$O$_5$) was stabler and released fewer ions in fluorinated Fusayama solution. Furthermore, the addition of Zr to

titanium alloys' chemical composition improves chemical resistance due to oxide layer formation (ZrO$_2$) [9].

The titanium alloys employed for prostheses present a longer lifetime expectancy of over 20 years. During this period of time, alloys may endure corrosion, a hydrolysis phenomenon that modifies the passive oxide layer and changes the pH of surrounding media [4]. These changes in the environment can generate potential differences that accelerate the corrosion rate on titanium alloy surfaces. As corrosion resistance plays an important role in titanium alloys' biocompatibility, the *in vitro* evaluation is one of the first steps to evaluate their suitability for biomedical applications. Regardless of their chemical composition, all titanium alloys present phenomes corrosion that releases ions to the surrounding environment. This section summarizes the quantification results obtained for the ions released from Ti—35Nb—7Zr—5Ta as measured by ICP-OES. The characterization of the etched surface by fluorinated Fusayama solution was evaluated by optical microscopy.

Microstructure, chemical and phase compositions are the main sources for titanium alloys' biocompatibility, and are related to their surface integrity, corrosion resistance and ion release. Davis et al. (2003) concluded that the metal ion concentration threshold for cell viability with bulk metals was 15.5 μg/L for Ti, 8.5 μg/L for Mo and 172.0 μg/L for Nb. The present study demonstrated that the HIPed powder metallurgic processing route gave low metal ion release values (Fig. 8) in a scenario that simulated 20 years of corrosion, which indicates that this technology is suitable for obtaining beta titanium alloys with low cytotoxicity [26].

Selective alpha phase dissolution was noted in the samples, as observed by the formation of cavities on grain boundaries and in α+ β colonies (Fig. 7). The increment in α + β phase regions increased the element ion release of Ti—35Nb—7Zr—5Ta alloys (Fig. 8). The fast-cooling HIPed samples (HIP 1) released a significantly lower ion concentration to the solution compared to their low cooling HIPed counterparts (HIP 2).

As previously mentioned, the addition of beta stabilizer elements (Nb, Ta, Mo) resulted in a stabler pentoxide layer on the titanium surface, which reduced metal ion release to media [4,5,7,9,27]. Taken together, these main alloying elements added to the titanium alloy led to less metallic ion release, which makes beta titanium alloys more biocompatible than the conventional Ti6Al4V ELI or NiTi ones currently employed with medical devices [28].

Table 6 — The electrochemical impedance parameters obtained by the EEC for the conventional pressed and sintered HIPed samples.

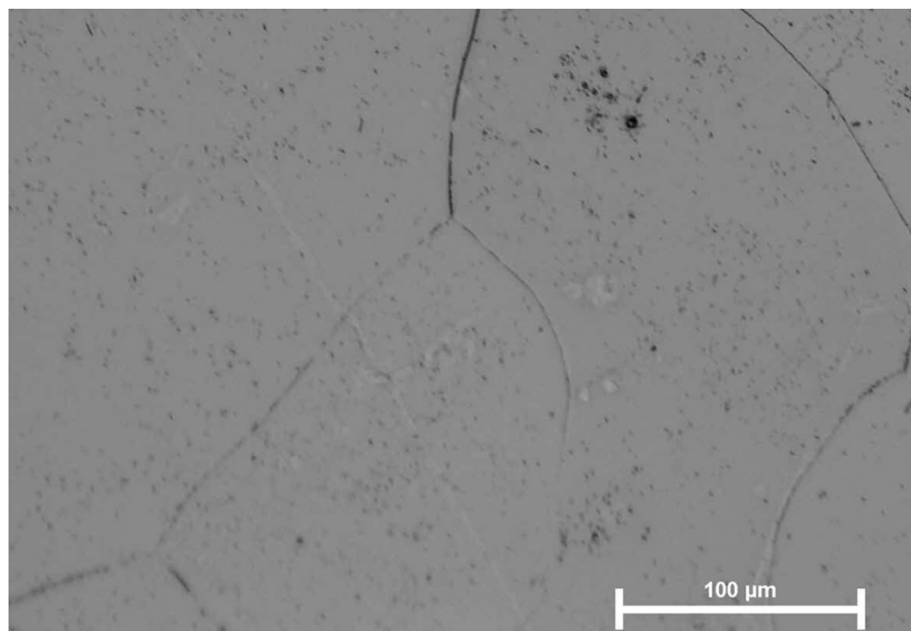| Composition	Processing condition	Rs ($\Omega\cdot$cm^2)	R1 ($\Omega\cdot$cm^2)	Q1 (F$\cdot$ cm^2)	n1	R2 x10^6 (Ω cm^2)	Q2 (F$\cdot$ cm^2)	n2	χ^2
Ti—35Nb—7Zr—5Ta	Press and Sintering (PS)	154 ± 47	407 ± 22	12.56 ± 0.38	0.92 ± 0.02	1.79 ± 0.71	3.72 ± 0.21	0.91 ± 0.01	0.002 ± 0.001
	HIP 1 (Fast cooling)	156 ± 9	750 ± 598	9.44 ± 0.33	0.93 ± 0.01	2.46 ± 0.31	1.42 ± 0.09	0.92 ± 0.01	0.007 ± 0.002
	HIP 2 (Slow cooling)	121 ± 35	207 ± 128	7.14 ± 0.11	0.91 ± 0.03	4.09 ± 2.45	1.96 ± 0.84	0.91 ± 0.01	0.003 ± 0.001

Figure 7 — Metallography of Ti—35Nb—7Zr—5Ta after 730 h of immersion in fluorinated Fusayama solution.
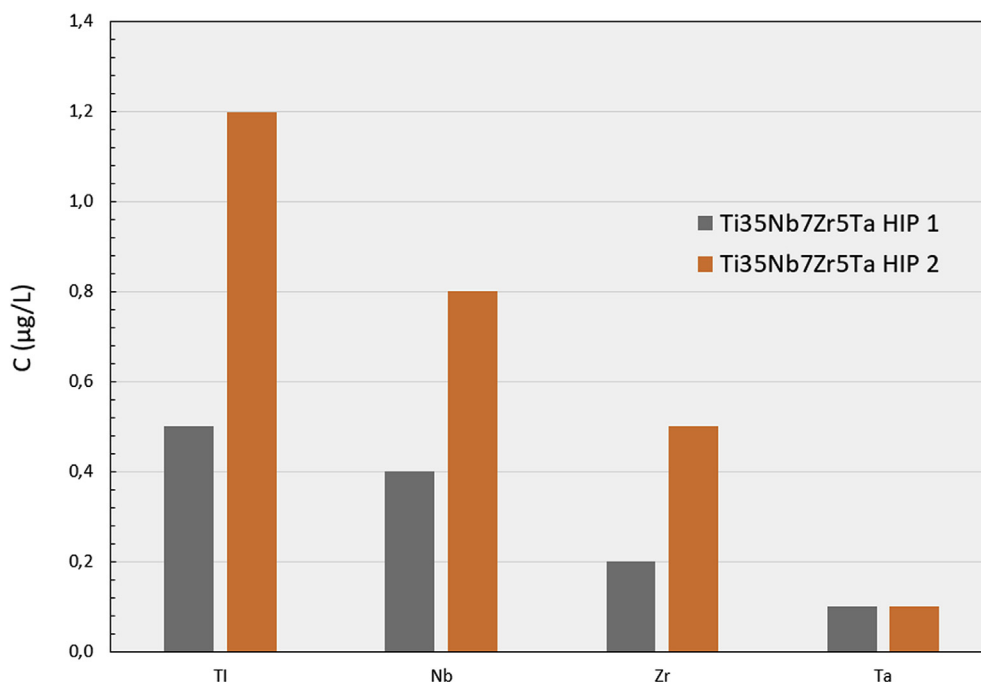

Fig. 8 — Metal ion concentration after 730 h of immersion in fluorinated Fusayama solution.

The nature of the titanium oxide layer (amorphous or crystalline) depends on how the passive film is obtained (heat oxidation, electrochemical, spontaneous), and also on the employed conditions, such as temperature, electrochemical potential, dissolution composition and atmosphere [29,30]. Two different paths should be followed for further beta titanium alloy development: reducing grain size to the nanoscale by the thermomechanical process [15,16,31]; electrochemical surface treatments followed by thermal post-processing to increase thickness and to obtain the anatase or rutile crystalline phase for titanium oxides [32].

4.　Conclusion

The thermo-mechanical process performed by HIP obtained the full density of the powder metallurgy Ti—35Nb—7Zr—5Ta alloys. The fast-cooling rate, 500 °C/min and set during HIP

post-processing, showed that a metastable β-type Ti35Nb7Zr5Ta alloy can be obtained by the powder metallurgy approach. The electrochemical measurements taken on fluorinated artificial saliva revealed that the HIPed Ti−35Nb−7Zr−5Ta samples presented a highly passive oxide layer, and released fewer ions than conventional Ti CP or Ti6Al4V ELI alloys. A high cooling rate during HIP thermomechanical treatment reduced the galvanic coupling effect on the Ti−35Nb−7Zr−5Ta alloys and improved passive film protectiveness. The higher beta phase percentage improved capacitive behavior by releasing a significantly lower ion concentration to solution. Therefore, the thermo-mechanical treatments influenced beta titanium alloys' biocompability. Further *in vitro* studies should be performed to determine the cell proliferation and viability of these new PM titanium alloys to determine their degree of osteocompability.

Funding

Declaration of Competing Interest

The authors declare that they have no known competing financial interests or personal relationships that could have appeared to influence the work reported in this paper.

Acknowledgments

REFERENCES

[1] Toumelin-Chemla F, Rouelle F, Burdairon G. Corrosive properties of fluoride-containing odontologic gels against titanium. J Dent 1996;24(1—2):109—15. https://doi.org/10.1016/0300-5712(95)00033-X.

[2] Schiff N, Grosgogeat B, Lissac M, Dalard F. Influence of fluoride content and pH on the corrosion resistance of titanium and its alloys. Biomaterials 2002;23(9):1995—2002. https://doi.org/10.1016/S0142-9612(01)00328-3.

[3] Huang GY, Jiang HB, Cha JY, Kim KM, Hwang CJ. The effect of fluoride-containing oral rinses on the corrosion resistance of titanium alloy (Ti-6Al-4V). Korean J Orthodontics 2017;47(5):306—12. https://doi.org/10.4041/kjod.2017.47.5.306.

[4] Manam NS, Harun WSW, Shri DNA, Ghani SAC, Kurniawan T, Ismail MH, et al. Study of corrosion in biocompatible metals for implants: a review. J Alloys Compd 2017;701:698—715. https://doi.org/10.1016/j.jallcom.2017.01.196.

[5] Rosalbino F, Delsante S, Borzone G, Scavino G. Influence of noble metals alloying additions on the corrosion behaviour of titanium in a fluoride-containing environment. J Mater Sci Mater Med 2012;23(5):1129—37. https://doi.org/10.1007/s10856-012-4591-9.

[6] Li Y, Xu J. Is niobium more corrosion-resistant than commercially pure titanium in fluoride-containing artificial saliva? Electrochim Acta 2017;233:151—66. https://doi.org/10.1016/j.electacta.2017.03.015.

[7] Zhou YL, Niinomi M, Akahori T, Fukui H, Toda H. Corrosion resistance and biocompatibility of Ti-Ta alloys for biomedical applications. Mater Sci Eng A 2005;398(1—2):28—36. https://doi.org/10.1016/j.msea.2005.03.032.

[8] Hussein AH, Gepreel MAH, Gouda MK, Hefnawy AM, Kandil SH. Biocompatibility of new Ti-Nb-Ta base alloys. Mater Sci Eng C 2016;61:574—8. https://doi.org/10.1016/j.msec.2015.12.071.

[9] Atapour M, Pilchak AL, Frankel GS, Williams JC. Corrosion behavior of β titanium alloys for biomedical applications. Mater Sci Eng C 2011;31(5):885—91. https://doi.org/10.1016/j.msec.2011.02.005.

[10] Vasilescu C, Drob SI, Neacsu EI, Mirza Rosca JC. Surface analysis and corrosion resistance of a new titanium base alloy in simulated body fluids. Corrosion Sci 2012;65:431—40. https://doi.org/10.1016/j.corsci.2012.08.042.

[11] Cui C, Hu BM, Zhao L, Liu S. Titanium alloy production technology, market prospects and industry development. Mater Des 2011;32(3):1684—91. https://doi.org/10.1016/j.matdes.2010.09.011.

[12] Calderon Moreno JM, Vasilescu E, Drob P, Osiceanu P, Vasilescu C, Drob SI, et al. Surface analysis and electrochemical behavior of Ti-20Zr alloy in simulated physiological fluids. Mater Sci Eng B: Solid-State Mater Adv Technol 2013;178(18):1195—204. https://doi.org/10.1016/j.mseb.2013.07.006.

[13] Torralba JM, Campos M. Toward high performance in Powder Metallurgy. Rev Metal (Madr) 2014;50(2). https://doi.org/10.3989/revmetalm.017.

[14] Schroeder HA, Balassa JJ, Tipton IH. Abnormal trace metals in man—Vanadium. J Chron Dis 1963;16:1047—71. https://doi.org/10.1016/0021-9681(63)90041-9 [- DOI - PubMed].

[15] Zherebtsov SV, Dyakonov GS, Salem AA, Malysheva SP, Salishchev GA, Semiatin SL. Evolution of grain and subgrain structure during cold rolling of commercial-purity titanium. Mater Sci Eng A 2011;528(9):3474—9. https://doi.org/10.1016/j.msea.2011.01.039.

[16] Kim HS, Yoo SJ, Ahn JW, Kim DH, Kim WJ. Ultrafine grained titanium sheets with high strength and high corrosion resistance. Mater Sci Eng A 2011;528(29—30):8479—85. https://doi.org/10.1016/j.msea.2011.07.074.

[17] Yılmaz E, Gökçe A, Findik F, Gulsoy HO, İyibilgin O. Mechanical properties and electrochemical behavior of porous Ti-Nb biomaterials. J Mech Behav Biomed Mater 2018;87(May):59—67. https://doi.org/10.1016/j.jmbbm.2018.07.018.

[18] Lario-Femenía J, Amigó-Mata A, Vicente-Escuder Á, Segovia-López F, Amigó-Borrás V. Desarrollo de las aleaciones de titanio y tratamientos superficiales para incrementar la vida útil de los implantes. Rev Metal (Madr) 2016;52(4):84. https://doi.org/10.3989/revmetalm.084.

[19] Levy Milton. Anodic behavior of titanium and commercial alloys in sulfuric acid. Corrosion 1967;23(8):236—44. https://doi.org/10.5006/0010-9312-23.8.236 (1967).

[20] Raducanu D, Vasilescu E, Cojocaru VD, Cinca I, Drob P, Vasilescu C, et al. Mechanical and corrosion resistance of a new nanostructured Ti-Zr-Ta-Nb alloy. J Mech Behav Biomed Mater 2011;4(7):1421—30. https://doi.org/10.1016/j.jmbbm.2011.05.012.

[21] Yılmaz E, Gökçe A, Findik F, Gulsoy Ho O. Metallurgical properties and biomimetic HA deposition performance of Ti-Nb PIM alloys. J Alloys Compd 2018;746:301−13. https://doi.org/10.1016/j.jallcom.2018.02.274.

[22] Wang BL, Zheng YF, Zhao LC. Electrochemical corrosion behavior of biomedical Ti e 22Nb and Ti e 22Nb e 6Zr alloys in saline medium. Mater Corros 2009:788e794. https://doi.org/10.1002/maco.200805173.

[23] Martins DQ, Os_orio WR, Souza MEP, Caram R, Garcia A. Effects of Zr content on microstructure and corrosion resistance of Ti-30Nb-Zr casting alloys for biomedical applications. Electrochim Acta 2008;53:2809e2817. https://doi.org/10.1016/j.electacta.2007.10.060.

[24] Hwang MJ, Choi HR, Kook MS, Song HJ, Park YJ. Investigation of passivation and galvanic corrosion of Ti-Nb alloys and pure titanium. Mater Corros 2014:783e789. https://doi.org/10.1002/maco.201407784.

[25] Mareci D, Ungareanu G, Aelenei DM, Mirza Rosca JC. Electrochemical characteristics of titanium based biomaterials in artificial saliva. Mater Corros 2007;58(11):848−56. https://doi.org/10.1002/maco.200704065.

[26] Davis JR, editor. Handbook of materials for medical devices. Ohio, USA: ASM International; 2003, ISBN 0-87170-790-X.

[27] Li Y, Wong C, Xiong J, Hodgson P, Wen C. Cytotoxicity of titanium and titanium alloying elements. J Dent Res 2010;89(5):493−7. https://doi.org/10.1177/0022034510363675.

[28] Cremasco A, Os WR, Freire MA, Garcia A, Caram R. Electrochemical corrosion behavior of a Ti-35Nb alloy for medical prostheses. Electrochim Acta 2008;53:4867−74. https://doi.org/10.1016/j.electacta.2008.02.011. 2008.

[29] Roguska A, Pisarek M, Belcarz A, Marcon L, Holdynski M, Andrzejczuk M, et al. Improvement of the bio-functional properties of TiO2 nanotubes. Appl Surf Sci 2016;388:775−85. https://doi.org/10.1016/j.apsusc.2016.03.128.

[30] Berger S, Hahn R, Roy P, Schmuki P. Self-organized TiO2 nanotubes: factors affecting their morphology and properties. Physica Status Solidi (B) Basic Research 2010;247(10):2424−35. https://doi.org/10.1002/pssb.201046373.

[31] Lario J, Viera M, Vicente Á, Igual A, Amigó V. Corrosion behaviour of Ti6Al4V ELI nanotubes for biomedical applications. J Mater Res Technol 2019;8(6):5548−56. https://doi.org/10.1016/j.jmrt.2019.09.023.

[32] Zhang Y, Figueiredo RB, Alhajeri SN, Wang JT, Gao N, Langdon TG. Structure and mechanical properties of commercial purity titanium processed by ECAP at room temperature. Mater Sci Eng A 2011;528(25−26):7708−14. https://doi.org/10.1016/j.msea.2011.06.054.